

LVS-Net: A Lightweight Vessels Segmentation Network for Retinal Image Analysis

Mehwish Mehmood, Shahzaib Iqbal *Member, IEEE*, Tariq Mahmood Khan *Member, IEEE*, Ivor Spence and Muhammad Fahim

Abstract—The analysis of retinal images for the diagnosis of various diseases is one of the emerging areas of research. Recently, the research direction has been inclined towards investigating several changes in retinal blood vessels in subjects with many neurological disorders, including dementia. This research focuses on detecting diseases early by improving the performance of models for segmentation of retinal vessels with fewer parameters, which reduces computational costs and supports faster processing. This paper presents a novel lightweight encoder-decoder model that segments retinal vessels to improve the efficiency of disease detection. It incorporates multi-scale convolutional blocks in the encoder to accurately identify vessels of various sizes and thicknesses. The bottleneck of the model integrates the Focal Modulation Attention and Spatial Feature Refinement Blocks to refine and enhance essential features for efficient segmentation. The decoder upsamples features and integrates them with the corresponding feature in the encoder using skip connections and the spatial feature refinement block at every upsampling stage to enhance feature representation at various scales. The estimated computation complexity of our proposed model is around 29.60 GFLOP with 0.71 million parameters and 2.74 MB of memory size, and it is evaluated using public datasets, that is, DRIVE, CHASE_DB, and STARE. It outperforms existing models with dice scores of 86.44%, 84.22%, and 87.88%, respectively.

I. INTRODUCTION

THE retina, a morphological and functional extension of the brain, is part of the neurological system; some of its cells directly connect to the brain [1], [2], [3], [4], [5]. Retinal blood vessels are the only vascular network in the human body that is directly and non-invasively observable [6], [7], [8], [9], [10]. Retinal vascular structural abnormalities are significant for their clinical implications in identifying systemic and neurological disorders, including dementia, such as Alzheimer’s disease [11], [12], [13], [14], [15]. This has led to a growing interest in investigating how early Alzheimer’s disease causes retinal changes, as retinal vessel health may reflect the cerebral vasculature’s condition due to the homology between the retina and the cerebral microvasculature [16]. An estimated 16 million people worldwide are affected by retinal vascular conditions, with Alzheimer’s being the second most common retinal vascular condition after diabetic retinopathy [17], [18], [19], [20], [21].

Mehwish Mehmood, Muhammad Fahim, and Ivor Spence are currently working with School of Electronics, Electrical Engineering and Computer Science, Queen’s University Belfast, UK (e-mail: mmehmood01@qub.ac.uk, m.fahim@qub.ac.uk, i.spence@qub.ac.uk).

Shahzaib Iqbal is working with the Department of Computing, Abasyn University, Islamabad, Pakistan (e-mail: shahzeb.iqbal@abasynisb.edu.pk).

Tariq Mahmood Khan is with the School of Computer Science and Engineering, University of New South Wales, Sydney, Australia

Medical image segmentation plays a crucial role in health-care by enabling precise delineation of anatomical structures and pathological regions, which aids in disease diagnosis, treatment planning, and monitoring [22], [23], [24], [25], [26], [27], [28]. Fundus imaging offers a non-invasive and efficient means of studying the cerebral microvasculature and its relationship to dementia. Retinal images are easy to acquire and growing evidence suggests that this microvascular network may represent the cerebral microvasculature [29], [30], [31]. Retinal image analysis has been dramatically improved by the development of image processing and machine learning technologies, which have improved disease diagnosis and monitoring [32], [33], [34], [35], [36], [37], [38]. The retinal vascular segmentation of these images is essential for monitoring anatomical changes and possibly diagnosing diseases like Alzheimer’s. Retinal image analysis is tedious as their color or gray level varies from one part to another due to the morphology of the retinal structure and different features, resulting in inaccurate output.

Retinal vascular segmentation remains challenging despite advancements, particularly in terms of vessel distinction [39], [40], [41], [42], [43], [44], [45]. This research introduces LVS-Net, a novel lightweight encoder-decoder model that improves the effectiveness of disease screening by segmenting retinal vessels. Our proposed lightweight model integrates the Focal Modulation Attention Module (FMAM) [46] and the spatial feature refinement block (SFRB) [47] into the bottleneck to refine and improve essential features for efficient segmentation. The decoder upsamples features and integrates them with the corresponding feature in the encoder using skip connections and SFRB to enhance feature representation at various scales and to fine-tune the segmented image’s overall representation. The suggested model is evaluated on public datasets, that is, DRIVE [48], CHASE_DB [49], and STARE [50]. The results show a notable improvement in retinal vascular segmentation over existing accuracy, efficiency, and complexity methods.

The primary contributions of this paper include:

- Introducing LAV-Net, a novel lightweight encoder-decoder model specifically designed for segmentation of retinal vessels. LAV-Net is highly effective and performs exceptionally well with a relatively small number of learnable parameters (only 0.71M).
- Implementing multi-class segmentation to identify arteries and veins from retinal images, facilitating the model to retrieve multiple features simultaneously while improving efficiency.
- Integrating focal modulation attention and spatial feature refinement blocks at the encoder-decoder bottleneck to

refine important features guarantees that more detailed information is transferred for efficient segmentation. Crucial details are maintained and improved during the decoding process by introducing SFRB in the decoder block that combines robust upsampling techniques with feature aggregation.

The paper is organized as follows: Section II contains the work related to retinal vessel segmentation. The methodology of the suggested model is described in Section III. The experiments and findings are covered in Section IV. Lastly, Section V contains the conclusion.

II. RELATED WORK

In the past few years, deep learning-based techniques are common for segmenting retinal blood vessels and have outstanding accuracy that suppressed traditional segmentation methods. The recent advancement in this area is discussed below.

A. Retinal Vessel Segmentation

Chowdhury *et al.* [51] developed MSGANet-RAV, a U-shaped encoder-decoder network that segments and classifies retinal vessels. Although it performed well, particularly in handling vessel crossings, it still demonstrated limitations in accurately segmenting small vessels and other detailed structures. Hemelings *et al.* [52] utilized a U-Net architecture, achieving high accuracy, but leaving room for improvement in the discrimination of small vessels. Lyu *et al.* [53] presented a convolutional neural network (CNN) model comparable to U-Net for the segmentation of binary vessels and the assessment of fractal dimensions. Xu *et al.* [54] proposed a dual channel asymmetric CNN based on the U-Net model based on pre-processing scale and orientation features. The combination of the segmentation results from both channels resulted in comprehensive and complementary information. However, the effectiveness of these techniques is limited by the pathological variability present in clinical images and the various scales of vascular geometry. Additionally, these variations may incorporate supplementary structural elements, leading to a higher number of network learnable parameters and, as a result, increased GPU memory consumption.

Unlike CNN-based architectures, transformers have recently been adopted in many computer vision tasks. Vision transformers (ViTs) [55] have received a substantial research interest, and various subsequent approaches have been presented that expand on ViTs. They adjusted the architecture by cascading numerous transformer layers instead of CNN-based architectures. Due to the powerful representation learned from pre-trained backbones, numerous algorithms for semantic segmentation that incorporate ViT backbones demonstrate impressive results [56], [57], [58], [59]. Although ViTs yield robust outcomes, they are computationally expensive.

Using lightweight CNNs is one potential way to overcome these problems. There are several advantages to using lightweight techniques in medical imaging, including faster processing speeds, lower memory requirements, better portability, lower computational costs, and lower power usage.

These advantages make them an attractive option for several applications, which has recently attracted the interest of most academics. Wentao *et al.* [60] introduce FR-UNet, a novel segmentation technique designed to improve segmentation accuracy and vessel connectivity. A dual-threshold iterative approach is used to capture weak vessel pixels, and the network retains full image resolution while enhancing feature extraction through a multiresolution convolution mechanism. FR-UNet tends to create false positives during the segmentation of thin vessels. The Dense-Inception U-Net was proposed by Zhang *et al.* [61], and utilizes a tiny encoder along with a lightweight backbone and dense module to capture high-level semantic information.

Several researchers have developed lightweight networks specifically for the segmentation of medical images. However, achieving minimal model complexity and rapid inference while maintaining outstanding performance remains challenging in medical imaging. NnU-Net [62] preprocesses the data and postprocesses the segmentation outcomes to boost network flexibility; however, this method increases the model parameters. The lightweight V-Net [63] allows for efficient segmentation and uses a lower number of parameters utilizing point-wise and depth-wise convolution; nevertheless, it fails to accelerate the inference process of the model. Furthermore, using multimodal magnetic resonance imaging (MRI), Tarasiewicz *et al.* [64] trained multiple tiny networks across all image channels to create lightweight U-Nets to precisely identify brain tumors. By replacing all convolutional layers in conventional U-Net with pyramidal convolution, PyConvU-Net [65] increases segmentation accuracy and requires a smaller number of parameters. Nevertheless, PyConvU-Net's inference time remains inadequate. CNN architectures that are lightweight and effective for segmenting retinal blood vessels are G-Net Light [43], PLVS-Net [44], TBConvL-Net [25], Lmbf-net [22] and MKIS-Net [45]. There are two significant drawbacks to existing lightweight methods. Firstly, they do not match the state-of-the-art methods in terms of performance, and secondly, they cannot generalize. Existing methods, including lightweight methods, unable to detect multi-retinal features with state-of-the-art results [66].

B. Retinal Arteries Veins Segmentation

Morano *et al.* [67] presented a novel approach that uses fully convolutional neural networks (FCNN) and a unique loss function of 'Binary cross entropy by 3' (BCE3) for simultaneous segmentation and classification of retinal arteries and veins. This approach performs exceptionally well in handling vessel crossings, but still has room for improvement. Shi *et al.* [68] present a novel one-shot method to segment the retinal arteries and veins that uses fundus fluorescein angiography (FFA) and color fundus photography (CFP) with cross-modal pre-training. This method trained a GAN to produce soft segmentation AV using CFP inputs. There is still a need for improvement, as the approach indicated a possible loss of small vessel information, even with its capacity to manage insufficient data. LUNet, a unique deep learning architecture for segmentation of the arteries

and veins in high-resolution fundus images, was introduced by J. Fhima *et al.* [69]. In order to improve the receptive field, the model has a particular double-dilated convolutional block. LUNet relies on high-quality images, which can affect segmentation accuracy in cases where image quality is poor. Despite good performance on high-resolution datasets, challenges in processing large-scale datasets and small vessels persisted.

Danli *et al.* presented the Retina-based microvascular health assessment system (RMHAS) using a multibranch U-Net to segment the optic disc, veins, and arteries. Real-time application may be limited by the multi-step RMHAS process, which includes image quality evaluation and multibranch segmentation. This procedure may also increase computational complexity and processing time. Jingfei Hu *et al.* [70] presented a novel multi-scale interactive network with an artery-venous (A/V) discriminator for classifying retinal arteries and veins. Using a special A/V discriminator, the network integrates multi-scale data and tackles common problems such as arteriovenous confusion and vascular discontinuity. Real-time implementation may be constrained by the method's complexity in integrating multi-scale data and implementing an A/V discriminator, which could raise computing costs. Wenao Ma *et al.* [71] presented a network in which the input module integrates domain knowledge from widely utilized vessel enhancement and retinal preprocessing methods. Specifically created for the network output block, a spatial activation mechanism uses vessel segmentation to improve A/V classification performance. Deep supervision is also incorporated into the network to help lower layers extract valuable data. Pre-processing is a significant method component which could limit generalization to different datasets and increase model complexity.

Segmentation of retinal vessels has advanced significantly. However, there are still many challenges with the existing models. Real-time implementation is challenging due to the high memory requirements and the longer inference time of complex models, which are computationally intensive [72]. Although lightweight models have benefits such as reduced memory utilization and faster processing, they typically fail to incorporate complex processes like attention modules. This leads to a substantial gap in the development of lightweight models that incorporate attention processes for improved segmentation accuracy, particularly in the segmentation of retinal vessels [73].

III. METHODOLOGY

Our lightweight model is designed for the segmentation of retinal vessels with an encoder-decoder architecture. The images in the datasets used for model evaluation are limited in number. To address this issue, data augmentation is employed, which consists of rotating the images by 20 degrees and adjusting the contrast of the rotated images. The architecture of our proposed model is discussed in the following section.

A. Model Architecture

We present a lightweight encoder-decoder architecture, LVS-Net, to extract the retinal vessels from fundus images. The overall network architecture is depicted in Fig. 1, which introduces multi-scale analysis and feature refinement inside the model. To enhance channel mapping and fine-tune the details, this network's bottleneck layer uses focal modulation along with spatial feature enhancement. The proposed LVS-Net comprises skip connections to preserve the original information from the encoder and use it during the decoding process. The output of the 1st skip connection (S_1) is obtained by applying an activation function and a convolution operation on the RGB input image with 512×512 resolution, as given in Eq. 1.

$$S_1 = ReLU(C^{1 \times 1, 24}(Img_{512 \times 512})) \quad (1)$$

Here, the operation $C^{1 \times 1, 24}$ denotes a convolution with 1×1 kernel size and 24 output channels. $ReLU$ represents the activated Rectified Linear Unit (ReLU). The 1st convolution block employs an activation function after a 3×3 convolution operation on $Img_{512 \times 512}$. The resulting output is concatenated with (S_1), as shown in Eq. 2.

$$F_1 = ReLU(C^{3 \times 3, 24}(Img_{512 \times 512})) \oplus S_1 \quad (2)$$

Where \oplus is the concatenation operation. The 2nd skip connection employs a batch normalization on F_1 followed by a max-pooling layer to reduce the spatial dimensions, as shown in Eq. 3.

$$S_2 = MaxPool_{2 \times 2}(BN(F_1)) \quad (3)$$

Where BN is the batch normalization. The 2nd convolution block and the 3rd skip connection are mathematically represented in Eq. 4 and Eq. 5, respectively.

$$F_2 = Re(C^{1 \times 1, 48}(S_2)) \oplus ReLU(C^{3 \times 3, 48}(S_2)) \quad (4)$$

$$S_3 = MaxPool_{2 \times 2}(BN(F_2)) \quad (5)$$

Finally, the 3rd convolution block and 4th skip connection are presented in Fig. 6 and Eq. 7, respectively.

$$F_3 = ReLU(C^{1 \times 1, 96}(S_3)) \oplus ReLU(C^{3 \times 3, 96}(S_3)) \quad (6)$$

$$S_4 = Dr^{(0.5)}(MaxPool_{2 \times 2}(BN(F_3))) \quad (7)$$

Where $D^{(0.5)}$ is the dropout operation with a probability of 0.5. The proposed LVS-Net applies the FMAM to refine the encoded features and improve the channel mapping after using max-pooling layers. Once the encoder features are refined by FMAM, they are processed through SFRB and then concatenated with the actual information using skip connection to compute the output of the decoder block 1st as shown in Eq. 8.

$$D_1 = \mathcal{G}(\mathcal{F}(S_4)) \oplus S_4 \quad (8)$$

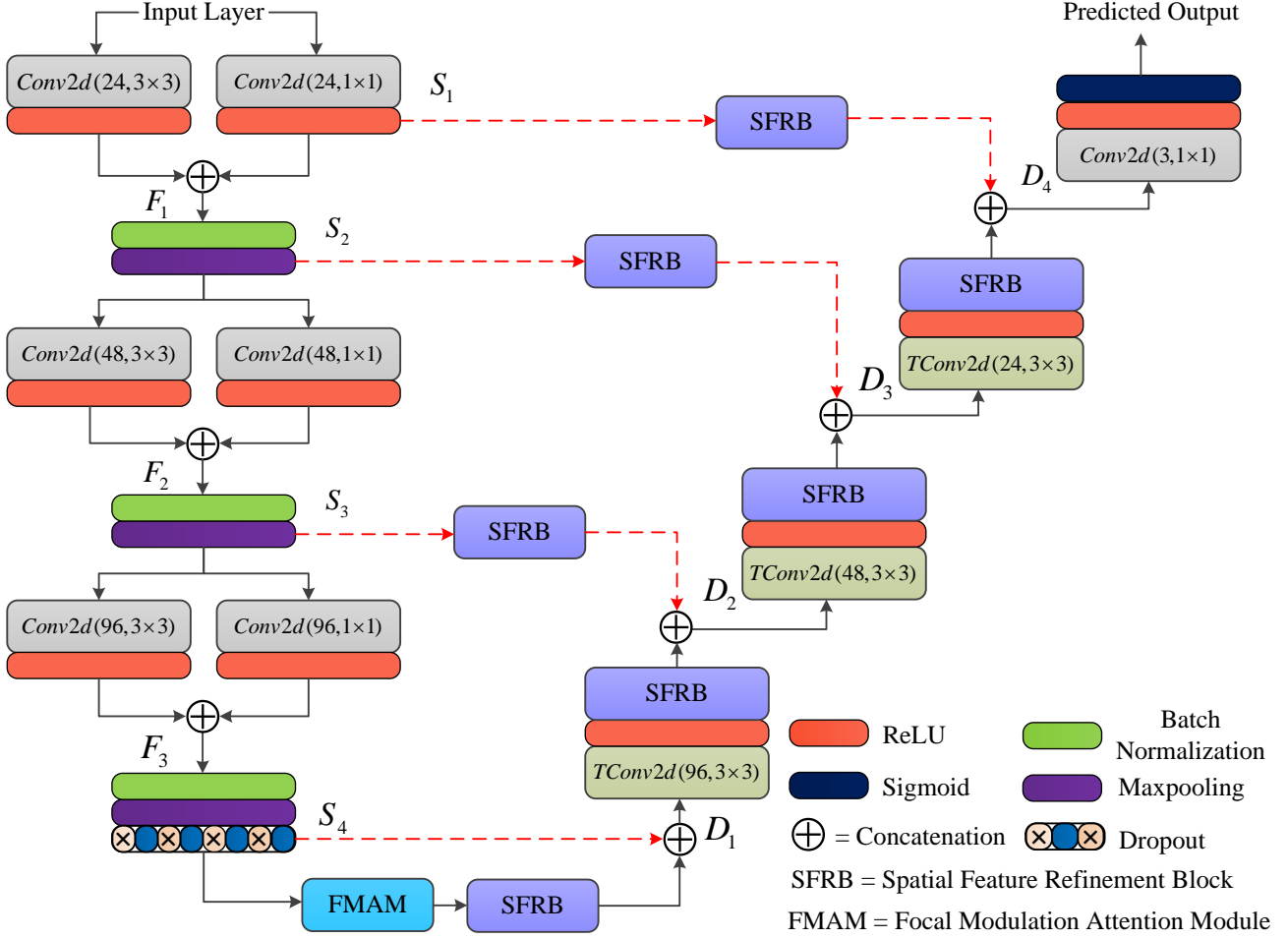


Fig. 1. Architecture of the proposed LVS-Net: begins with convolutional operations followed by a decoding path using transposed convolutions. Key elements include Focal Modulation Attention and Spatial Feature Refinement block in various stages of model for precise segmentation.

Where, SFRB and FMAM are denoted as \mathcal{G} and \mathcal{F} , respectively.

A transposed convolution operation is applied to D_1 to up-sample feature maps, followed by a ReLU activation and SFRB to enhance spatial features. Subsequently, the feature maps are concatenated with the output of SFRB applied to S_3 to preserve the original information as shown in Eq. 9.

$$D_2 = \mathcal{G}(\text{ReLU}(T^{3 \times 3, 96}(D_1))) \oplus \mathcal{G}(S_3) \quad (9)$$

Where the operation $T^{3 \times 3, 96}$ denotes a transposed convolution with 3×3 kernel size and 96 output channels. The output of the 3rd and 4th decoder blocks (D_3 and D_4) are calculated as Eqs. 10 - 11

$$D_3 = \mathcal{G}(\text{ReLU}(T^{3 \times 3, 48}(D_2))) \oplus \mathcal{G}(S_2) \quad (10)$$

$$D_4 = \mathcal{G}(\text{ReLU}(T^{3 \times 3, 24}(D_3))) \oplus \mathcal{G}(S_1) \quad (11)$$

The final predicted mask is computed by applying 1×1 convolution operation, followed by a ReLU activation and sigmoid function, as shown in Eq. 12.

$$I_{out} = \sigma(\text{ReLU}(C^{1 \times 1, 1}(D_4))) \quad (12)$$

Where σ is the sigmoid operation. To convert the predicted map from the decoder to a segmentation mask, F1-thresholding is used that maximizes the dice score. Furthermore, the dice loss function and Adam optimizer are used to train our model. Dice loss measures what percentage of overlap occurs between the segmented image S and the ground truth (GT) image G :

$$\mathcal{L}_d(S, G) = 1 - \sum_{k=1}^c w_k \frac{2 \sum_{j=1}^n S(k, j) \cdot G(k, j)}{\sum_{j=1}^n S(k, j)^2 + \sum_{j=1}^n G(k, j)^2 + \xi} \quad (13)$$

where w_k represents the weight of the k -th class, c , n and ξ are the number of pixels, the number of classes, and a smoothing constant, respectively.

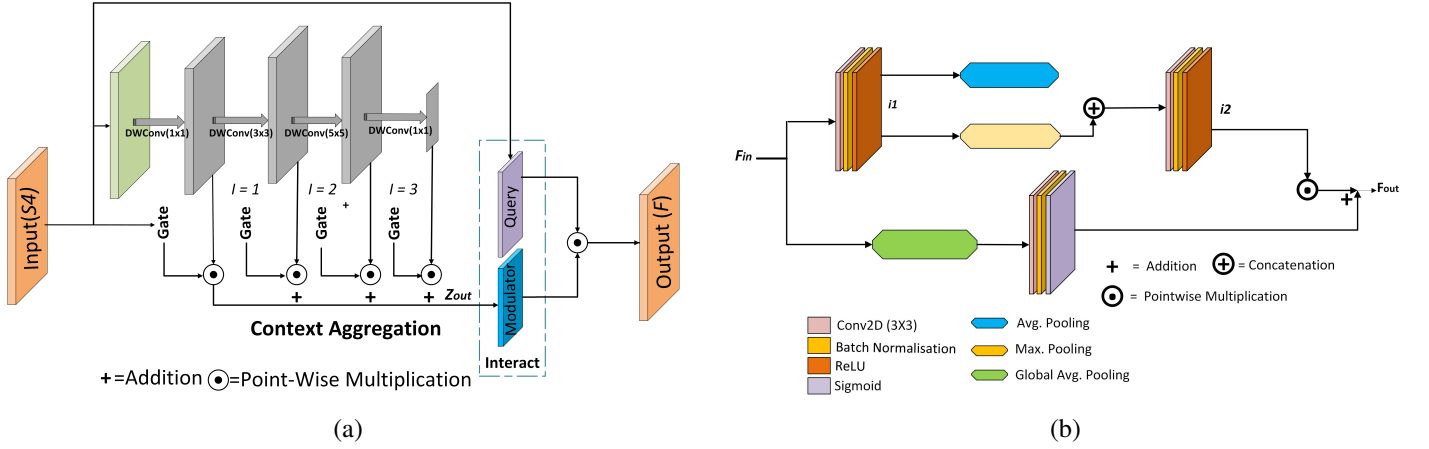


Fig. 2. Schematics of the proposed blocks: (a) Focal modulation attention module with context aggregation, (b) Spatial feature refinement block.

B. Focal Modulation Attention Module

To further improve the obtained feature information, FMAM has been utilized between the encoder and the decoder. It is made up of three different elements, as Fig. 2(a) illustrates. It initially employs input from the encoder to encode the visual details at short and long ranges using a sequence of depth-wise convolutional layers. Each layer in the stack extracts various levels of information, including local and global details.

$$z^{(l)} = (\text{DWConv}(z^{(l-1)})) \quad (14)$$

Where $z^{(l)}$ is the output feature map at level (l) and DWConv is depth-wise convolution at level (l).

The global context is obtained as:

$$z^{L+1} = \text{AvgPool}(z^L) \quad (15)$$

It refines input features through hierarchical context aggregation and modulation. The aggregated context features across all levels are combined as:

$$Z_{\text{out}} = \sum_{(l)=1}^{L+1} G^{(l)} \odot z^{(l)} \quad (16)$$

where, $G^{(l)}$ is gating weights at level (l), and \odot is element-wise multiplication.

Using the context as guidelines, these extracted data are utilized later to collect context attributes for each query token in a selective manner. The significance of each contextual data in the final representation of the query token is determined by a gate with learnable attention weight. The modulated output for each query token F_i is computed as:

$$F_i = q(S4_i) \odot h(Z_{\text{out}}), \quad (17)$$

where i represents the spatial index in the feature map, $q(S4_i)$ is query projection function and $h(Z_{\text{out}})$ is modulator projection function. An element-wise multiplication is performed to fuse these combined context characteristics into the query token. A learnable weight matrix that is updated throughout the training defines this transformation.

C. Spatial Feature Refinement Block

Pooling operations are used to reduce model complexity and computational overhead. Max-pooling retains the dominant features, while average-pooling retains low-frequency features for global context. Parallel paths of the max-pooling and average-pooling operations are implemented in SFRB to integrate local and global features effectively.

In this approach, in Fig. 2(b), the input feature map F_{in} undergoes initial processing through convolutional layers, followed by batch normalization and ReLU activation represented in Eq. 18.

$$i_1 = \text{ReLU}(\text{BN}(C^{3 \times 3}(F_{in}))) \quad (18)$$

Subsequently, the results of the max-pooling $P_{\text{Max.}}^{3 \times 3}$ and average-pooling $P_{\text{Avg.}}^{3 \times 3}$ are concatenated, followed by convolution (C), batch normalization (BN) and ReLU activation (ReLU) calculated by Eq. 19.

$$i_2 = \text{ReLU}(\text{BN}(C^{3 \times 3}[P_{\text{Avg.}}^{3 \times 3}(i_1) \oplus P_{\text{Max.}}^{3 \times 3}(i_1)])) \quad (19)$$

Furthermore, an additional pathway is introduced that incorporates global average pooling ($P_{\text{Avg.}}^{\text{Global}}$), convolutional operations, batch normalization, and sigmoid activation function (Σ) to generate attention coefficients to weight the results of parallel pooling. Subsequently, the weighted feature map is combined with the input to produce the output F_{out} of SFRB, as shown in Eq.20.

$$F_{out} = [\sigma(\text{BN}(C^{3 \times 3}(P_{\text{Avg.}}^{\text{Global}}(F_{in})))) \odot i_2] + F_{in} \quad (20)$$

IV. EXPERIMENTS AND RESULTS

A. Datasets

Our model was evaluated on DRIVE, STARE, and CHASE_DB-DB datasets. There are forty colored retinal images in the DRIVE dataset [48], each with a resolution of 565×584 pixels (8 bits per channel). These images were taken with a Canon CR5 non-mydratic 3CCD camera with a 45-degree viewing field. Each of the two subsets of

the data set, the test set and the training set, consists of twenty images. Specifically, the test set benefits from two expert annotations, but the training set has access to one. STARE [50] dataset of retinal images widely employed in the development and evaluation of algorithms for the segmentation of retinal lesions. The Ophthalmic Image Analysis Laboratory created the University of California, Berkeley dataset. The STARE dataset includes retina scans of 13 different human eye diseases and a catalog of disease names and codes associated with each image. Manual expert annotations are available for the blood vessels and the optic nerve. It comprises 20 color fundus images with a 700×605 pixel resolution, acquired with a ‘‘Topcon TRV-50’’ camera. The images were obtained from patients with various retinal diseases and pre-processed to eliminate nonretinal areas. For each image, two independent expert graders provide ground-truth segmentation of retinal blood vessels. The CHASE_DB dataset [49] comprises 28 images, each with a resolution of 1024×1024 pixels. Scanning laser ophthalmoscopy (SLO) produces high-resolution retinal images, making these images distinctive. Each image in the CHASE_DB collection was captured using an EasyScan device (i-Optics Inc.) with a 45-degree field of view (FOV) that combines the SLO approach. A group of retinal image analysis professionals carefully annotated the vessels in this dataset.

B. Implementation Details

Our model is implemented in TensorFlow and Keras and an NVIDIA Tesla P100 GPU with 32 GB RAM is used to perform experiments with batch size 8. The model is also evaluated on multi-class segmentation, which performs retinal artery and vein segmentation from retinal images on the RITE dataset [74]. We employed 80% images for model training and 20% validation from each dataset.

C. Performance Metrics

Standard evaluation metrics, including accuracy, dice, jaccard, specificity, sensitivity, and area under the curve (AUC), are used to assess the model performance. Below are the specified evaluation metrics:

$$Accuracy(acc) = \frac{TP + TN}{TP + TN + FP + FN} \quad (21)$$

$$dice = \frac{TP + TP}{TP + TP + FP + FN} \quad (22)$$

$$Jaccard(J) = \frac{TP}{FN + FP + TP} \quad (23)$$

$$Sen = \frac{TP}{FN + TP} \quad (24)$$

$$Sp = \frac{TN}{FP + TN} \quad (25)$$

$$AUC = \frac{1}{2 \times TP \times TN} \sum_{i=1}^{TP} \sum_{j=1}^{TN} \left(1 + \frac{FN}{FP}\right) \quad (26)$$

where, false positive, true positive, false negative, and true negative are represented by FP, TP, FN, TN , respectively. Moreover, Sp and Sn represent specificity and sensitivity, respectively.

D. Performance Comparisons of the Blood Vessels Segmentation

The quantitative assessment of our suggested model is given in Table II along with other existing models. The table shows that LVS-Net outperforms existing techniques in several performance criteria, including sensitivity, specificity, accuracy, and dice score, while retaining the advantage of being lightweight. LVS-Net specifically achieved performance of 96.64%, 86.44%, 76.16%, 83.91%, and 98.51% for accuracy, dice, jaccard, sensitivity, and specificity on the DRIVE dataset. Similarly, on the STARE dataset, it achieved 97.59%, 84.78%, 71.56%, 85.19%, and 98.61% for accuracy, dice, jaccard, sensitivity, and specificity, respectively. In the CHASE_DB dataset, it achieved scores of 96.44%, 84.78%, 73.65%, 83.29%, and 98.44% for accuracy, dice, Jaccard, sensitivity, and specificity, respectively. These results show the superior performance of LVS-Net over other state-of-the-art models.

A clear assessment of the performance of the prediction algorithm is presented in Fig. 3 by marking true positives with green, false positives with red, and false negatives with blue. Visual inspection of the results in the DRIVE dataset reveals that the proposed LVS-Net yielded fewer false positives on thin vessels compared to the recent methods. Furthermore, the U-Net variants struggled with the boundaries (as depicted in image 4). SegNet generated false tiny vessels in most images, and G-Net Light tended to skip vessel information, which was robustly captured by LVS-Net while concealing inaccurate vessel information.

Similarly, inspection of the results in the STARE dataset Fig. 4, notably images 2 and 3) shows that the alternative methods produced more false positives, particularly across retinal boundaries, optic nerves, and tiny vessels. On the other hand, the proposed LVS-Net showed much more robustness to these artifacts in these images. Similar results can be observed from the results on the CHASE_DB dataset in Fig. 5.

In Fig. 6, the Receiver Operating Characteristic (ROC) curves are compared for three datasets, that is, DRIVE, STARE, and CHASE_DB, for various models together with our proposed model. Each figure displays the True Positive Rate (TPR) against the False Positive Rate (FPR). Outperforming the other models, the proposed model consistently obtains the highest AUC values across all datasets. In particular, the suggested model outperforms the existing models in terms of AUC with values of 0.993, 0.997, and 0.998 for DRIVE, STARE, and CHASE_DB, respectively.

E. Performance Comparisons of the AV Segmentation

This section evaluates the generalization of our model by performing retinal artery vein segmentation using the RITE dataset. The findings demonstrate that our model obtained a higher dice score compared to other models on the RITE dataset. Consequently, our model demonstrates performance comparable to that of existing models while maintaining the

TABLE I

OVERVIEW OF DATASETS AND THEIR PROPERTIES INCLUDING THE NUMBER OF TRAINING AND TESTING IMAGES, TOTAL AND AUGMENTED IMAGES, ORIGINAL IMAGE RESOLUTION, FIELD OF VIEW (FOV), AND TRAINING DETAILS PROVIDING BETTER INSIGHT INTO THEIR APPLICATION.

Feature	Dataset	Number of Images				Original Image		Training
		Training	Testing	Total	Augmented	Resolution	FOV	Details
Vessels	DRIVE [48]	20	20	40	720	565 × 584	35	Image Level
	CHASE_DB [49]	28	-	28	720	1024 × 1024	45	
	STARE [50]	20	-	20	720	700 × 605	45	
A/V	RITE[48]	20	20	40	720	565 × 584	35	

TABLE II

PERFORMANCE COMPARISON OF LVS-NET WITH RECENT METHODS ON THE DRIVE, STARE, AND CHASE_DB DATASETS. VARIOUS PERFORMANCE MEASURES ARE HIGHLIGHTED, INCLUDING ACCURACY, DICE COEFFICIENT, JACCARD INDEX, SENSITIVITY, AND SPECIFICITY, WITH THE BEST RESULTS EMPHASIZED IN BOLD FOR CLARITY.

Method	Param (M)	Performance Measures in (%)														
		DRIVE					STARE					CHASE_DB				
		Acc.	Dice	J	Sn	Sp	Acc.	Dice	J	Sn	Sp	Acc.	Dice	J	Sn	Sp
U-Net [75]	7.76	96.78	81.41	68.64	80.57	98.33	97.30	81.18	68.56	70.50	98.84	97.43	78.98	65.26	76.50	98.84
G-Net Light [43]	0.39	96.86	82.02	69.09	81.92	98.29	97.30	82.78	69.64	81.70	98.53	97.26	80.48	67.76	82.10	98.38
Att.Unet[76]	9.25	96.62	80.39	67.21	79.06	98.31	97.30	81.06	68.39	78.04	98.87	97.30	79.64	66.17	84.84	98.31
MultiResNet [77]	7.20	95.64	82.32	69.26	79.46	97.89	96.33	82.44	68.27	77.09	98.48	96.42	80.12	67.09	80.10	98.04
BCD-UNet [78]	20.65	95.75	82.49	69.33	79.84	98.03	96.34	82.30	68.14	78.92	98.16	96.18	79.32	67.42	77.35	98.01
SegNet [79]	1.42	95.81	83.02	70.23	80.18	98.26	96.72	83.41	70.71	80.12	98.65	96.78	81.96	68.56	81.38	98.24
U-Net++[80]	9.04	94.61	80.60	68.27	78.40	98.00	96.41	81.40	69.02	79.02	98.36	96.64	83.49	66.88	82.83	98.21
FR_UNet[60]	5.72	97.05	83.16	71.20	83.56	98.37	97.52	83.30	72.46	83.27	98.69	97.48	81.51	68.82	87.98	98.14
RetinaLiteNet [81]	0.066	95.07	80.60	70.50	78.40	98.00	95.25	80.87	71.03	78.32	98.04	95.57	78.53	67.32	73.12	97.92
LVS-Net	0.71	96.64	86.44	76.16	83.91	98.51	97.39	87.88	78.40	87.40	98.60	96.44	84.78	73.65	83.43	98.19

advantage of being lightweight.

Table III shows the performance of our model, and it is a comparison with existing state-of-the-art models tested on the RITE dataset. The table presents a comprehensive performance comparison of several retinal feature segmentation models, including UNet++, Att.Unet, BCD Unet, FR-UNet, RetinaLiteNet, and LVS-Net across the above mentioned datasets. The performance metrics evaluated are accuracy, dice coefficient, sensitivity, and specificity.

LVS-Net demonstrates comparable performance across all datasets with a small parameter count. In the RITE dataset, LVS-Net achieves an average value between arteries, veins, and the background of 97.54%, 81.34%, 81.30%, and 92.83% of accuracy, dice, sensitivity, and specificity, respectively. For better insight, we have reported the individual values of performance matrices for arteries and veins. These values are the performance measure between the arteries and the background for arteries and veins and the background for the veins. These results indicate its effectiveness in segmenting both arteries and veins, with significant improvements over other existing models.

LVS-Net consistently performs better than the other models on all datasets, demonstrating its reliability and accuracy in retinal arteries veins segmentation tasks. The equivalent values of performance matrices are attained by LVS-Net, demonstrated by the average performance metrics. These findings suggest that LVS-Net is an important tool in medical

imaging analysis, particularly well-suited for applications demanding accurate feature segmentation.

Our model consistently achieves higher accuracy and dice scores due to its more complex architecture, which effectively captures the vessels and identifies the arteries and veins in the retinal images. From the table, we can see that the lightweight characteristics of RetinaLiteNet reduced its ability to handle these complexities, resulting in performance degradation in multi-class problems.

The performance of traditional models UNet variants serves as a solid baseline, but the advances in models such as LVS-Net provide substantial improvements in vessel segmentation. The LVS-Net performance metrics are the most effective model for this task and offer a robust foundation and development in this domain for future research.

F. Ablation Study on DRIVE dataset

The ablation study, presented in Table IV, performed on the DRIVE dataset, provides insight into the effects of various components on model performance. Evaluate the addition of various components to the lightweight U-Net (LU) baseline model to determine how those components affect the final model. When multiscale layers (MLU) are integrated, overall performance metrics are slightly improved, starting with LU. CBAM is added to the skip connections of MLU, substantially improving specificity and accuracy, highlighting the importance of attention mechanisms. Performance is improved by implementing SFRB in skip

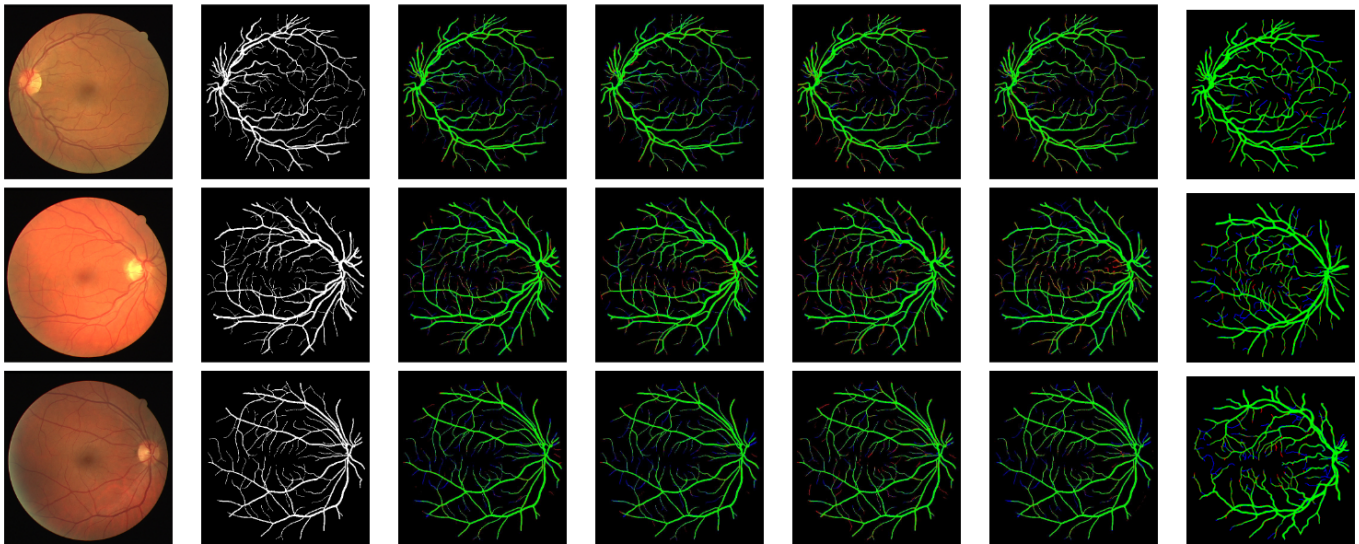


Fig. 3. Segmentation outcomes of selected test images from the DRIVE dataset. Arranged in a left-to-right sequence are the input images, specifically images 1, 2, and 19 from the dataset. Following the input images are the ground truth and the outputs of the G-Net Light, MultiResNet, SegNet, U-Net++, and LVS-Net models. True positives are shown with green color, red pixels represent false positive detections, whereas blue pixels indicate false negative detections.

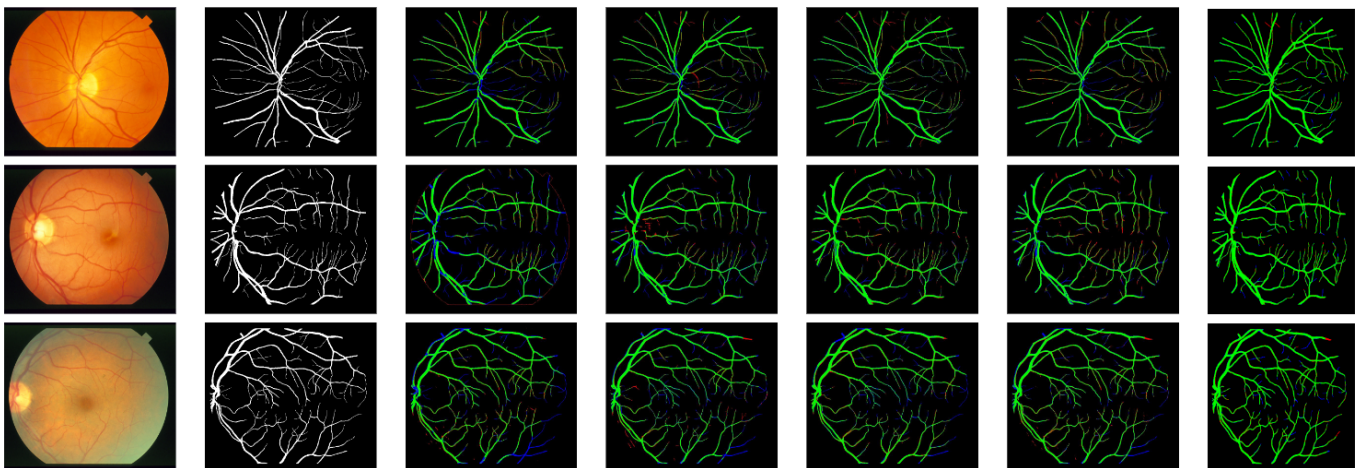


Fig. 4. Segmentation outcomes of selected test images from the STARE dataset. The images displayed in the following order are: input images (specifically images 2, 3, and 5 from the dataset). Following the input images are the ground truth and the outputs of the G-Net Light, MultiResNet, SegNet, U-Net++, and LVS-Net models. True positives are shown with green color, red pixels represent false positive detections, whereas blue pixels indicate false negative detections.

TABLE III

COMPREHENSIVE PERFORMANCE MATRIX COMPARISON OF LVS-NET AND OTHER EXISTING MODELS (U-NET++, ATT-UNET, BCD-UNET, FR_UNET, RETINALNET) ON THE RITE DATASET: ANALYSIS OF ACCURACY, DICE SCORE, SENSITIVITY, AND SPECIFICITY ACROSS ARTERIES, VEINS, AND OVERALL METRICS.

Dataset	Model	Performance Measures (%)											
		Arteries				Veins				Average			
		Acc.	Dice	Sn	Sp	Acc.	Dice	Sn	Sp	Acc.	Dice	Sn	Sp
RITE	UNet++ [80]	97.07	67.47	70.06	98.30	97.56	51.76	61.24	98.84	95.28	73.41	70.32	97.96
	Att.Unet [76]	97.10	73.54	72.06	98.78	97.46	63.66	68.83	98.08	95.72	78.29	70.99	97.89
	BCD-Unet [78]	97.11	71.00	69.98	98.76	97.67	66.77	68.25	97.68	94.87	76.24	69.29	97.55
	FR_Unet [60]	97.12	66.69	73.49	98.76	97.15	61.77	66.65	98.43	95.13	71.72	70.32	97.82
	RetinalNet [81]	97.05	74.55	71.32	98.70	97.51	70.11	70.57	98.41	94.50	70.12	71.82	97.91
	LVS-Net	97.13	75.46	73.52	99.95	99.75	71.18	75.48	98.44	98.44	81.34	81.83	99.21

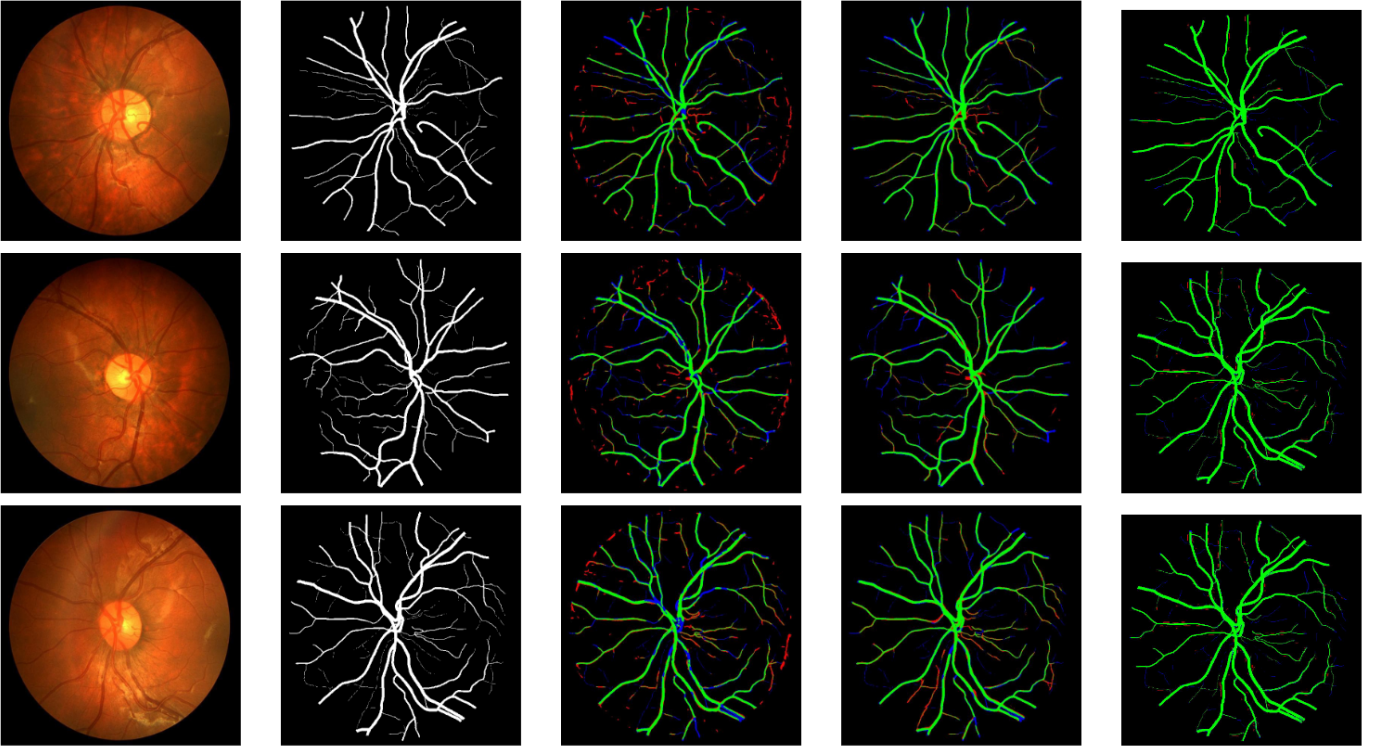


Fig. 5. Segmentation outcomes of selected test images from the CHASE_DB dataset [82]. Arranged horizontally, the images displayed are as follows: the input images (specifically, images 1, 2, and 3 from the dataset). Following the input images are the ground truth and the outputs of the G-Net Light, SegNet, and LVS-Net models. True positives are shown with green color, red pixels represent false positive detections, whereas blue pixels indicate false negative detections.

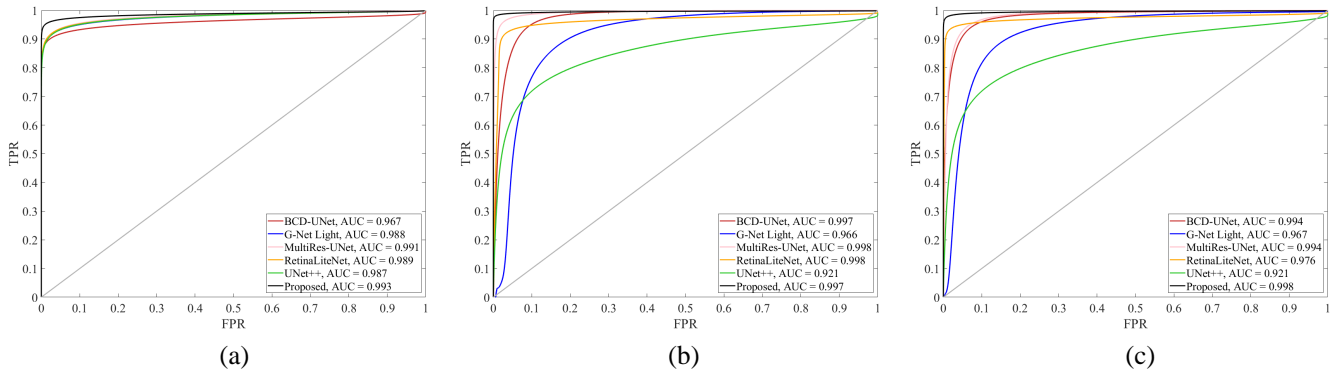


Fig. 6. Comparative Analysis of Receiver Operating Characteristic (ROC) Curves for Different Models Evaluated on Three Retinal Datasets: (a) DRIVE, (b) STARE, and (c) CHASE_DB with AUC Scores for BCD-UNet, G-Net Light, MultiRes-UNet, RetinalLightNet, UNet++ and LVS-Net.

connections and the bottleneck. The dice, jaccard, and sensitivity gradually increased. The ultimate model achieves the best performance across all metrics by implementing SFRB in skip connections and combining the components $SFRB(\mathcal{G})$ and $FMAM(\mathcal{F})$ on bottlenecks. These modifications indicate that the cumulative effect of these improvements significantly improves segmentation abilities.

The images in Fig. 7 visually demonstrate the impact of various components added to the proposed model. We can see that images (c), (d), and (e) depict results from Lightweight

U-Net (LU), Multiscale LU (MLU), and MLU with CBAM in Skip Connections, respectively, starting with (a) as the input RGB image and (b) as the ground truth. There are gaps in the vessel continuity and insufficient segmentation of the tiny vessels in these early models. Segmentation improves as we move on to images (f) and (g), which employ SFRB to skip connections and bottlenecks. Despite this, there is still some dilatation visible in the vessels. Using FMAM in the skip connections and bottleneck of images (h) and (i), the features of the vessel are further refined, capturing the delicate structures with less dilatation. The final image (j) obtains the optimal

TABLE IV
PERFORMANCE COMPARISON OF LVS-NET WITH VARIOUS RETINAL FEATURE SEGMENTATION MODELS ON RITE DATASET ACROSS DIFFERENT METRICS (ACCURACY, DICE SCORE, SENSITIVITY, AND SPECIFICITY) FOR ARTERIES, VEINS, AND COMBINED AVERAGES.

Method	Performance Measures (%)				
	Dice	J	Acc	Sen	Sp
Lightweight U-Net (LU)	82.06	66.29	96.09	82.20	98.04
Multiscale LU (MLU) (3×3 , 1×1)	83.49	68.57	96.52	83.63	98.47
MLU + CBAM in Skip Connections	80.86	67.53	95.80	78.42	97.41
MLU + (\mathcal{G}) in Skip Connections ((\mathcal{G})-Skip)	81.99	68.98	96.82	82.07	98.25
MLU + (\mathcal{G})-Skip + (\mathcal{G}) in Bottleneck ((\mathcal{G})-Bottleneck)	82.24	69.90	96.89	82.49	98.28
MLU + (\mathcal{F}) in Skip Connections ((\mathcal{F})-Skip)	82.25	70.23	95.96	81.48	97.42
MLU + (\mathcal{F}) in Bottleneck ((\mathcal{F})-Bottleneck)	83.81	73.11	96.17	83.18	97.77
MLU + (\mathcal{G})-Skip + (\mathcal{G})-Bottleneck + (\mathcal{F})-Bottleneck	86.44	76.16	96.64	83.91	98.51

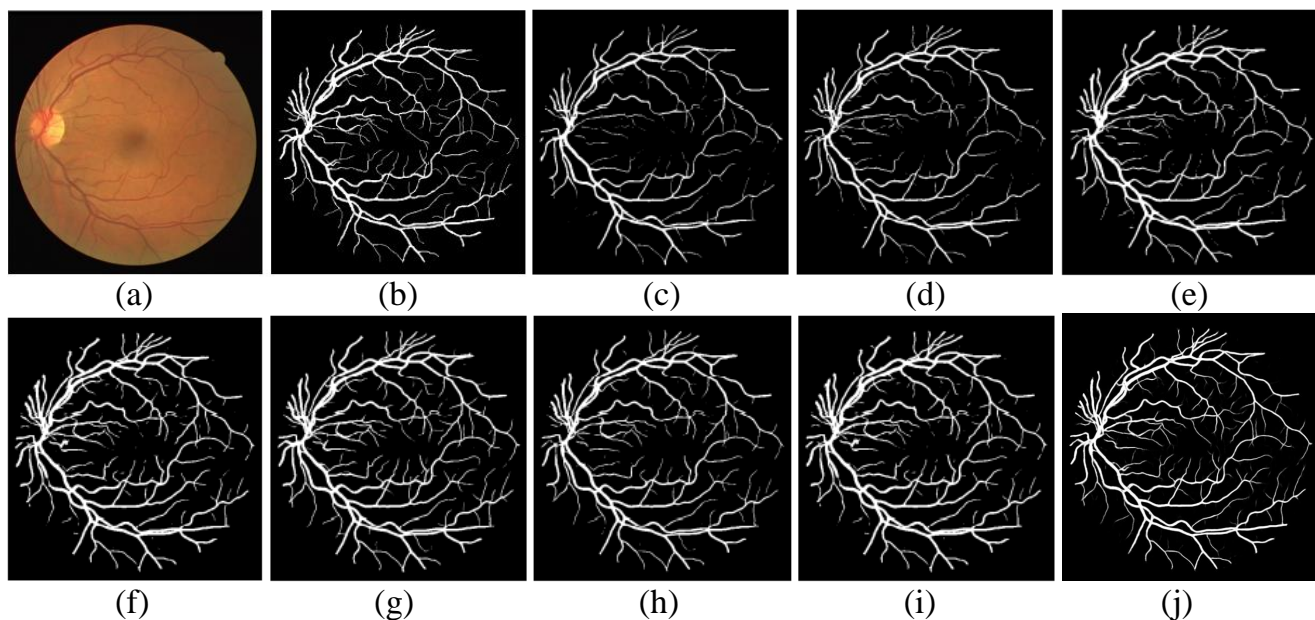


Fig. 7. Illustration of the visual results obtained by employing different components of the proposed architecture: (a) Input RGB image, (b) Corresponding ground-truth images, (c) Lightweight U-Net (LU), (d) Multiscale LU (MLU) (3×3 , 1×1), (e) MLU + CBAM in Skip Connections, (f) MLU + (\mathcal{G}) in Skip Connections ((\mathcal{G})-Skip), (g) MLU + (\mathcal{G})-Skip + (\mathcal{G}) in Bottleneck ((\mathcal{G})-Bottleneck), (h) MLU + (\mathcal{F}) in Skip Connections ((\mathcal{F})-Skip), (i) MLU + (\mathcal{F}) in Bottleneck ((\mathcal{F})-Bottleneck), and (j) MLU + (\mathcal{G})-Skip + (\mathcal{G})-Bottleneck + (\mathcal{F})-Bottleneck

segmentation result, which depicts the entire model with the integrated components of MLU, $SFRB(\mathcal{G})$, and $FMAM(\mathcal{F})$. It is identical to the ground truth and effectively captures the small vessels without dilation, which represents the efficiency of the proposed model.

V. CONCLUSION

In this paper, we introduce a lightweight encoder-decoder model based on the segmentation of retinal blood vessels. Our model comprises an encoder and decoder, embedding multi-scale convolutional layers with the combination of focal modulation attention and the spatial feature refinement

blocks at the bottleneck employed for the feature extraction. Furthermore, both the decoder and the skip connections use the spatial feature refinement block, helping to highlight and enhance key features. It is beneficial for image segmentation tasks where precise segmentation and localization of objects are important. Promising findings have been obtained from an extensive analysis of the model on public datasets, that is, DRIVE, CHASE_DB and STARE datasets, generating dice scores of 86.44%, 82.10% and 87.88%, respectively. Our model satisfies its lightweight requirements, 2.74 MB of memory, 0.71 million parameters, and 29.60 GFLOPs. These findings demonstrate that significant medical image analysis

persists and is feasible even with limited hardware resources.

REFERENCES

- [1] T. A. Soomro, M. A. Khan, J. Gao, T. M. Khan, M. Paul, and N. Mir, "Automatic retinal vessel extraction algorithm," in *2016 International Conference on Digital Image Computing: Techniques and Applications (DICTA)*. IEEE, 2016, pp. 1–8.
- [2] M. A. Khan, T. A. Soomro, T. M. Khan, D. G. Bailey, J. Gao, and N. Mir, "Automatic retinal vessel extraction algorithm based on contrast-sensitive schemes," in *2016 International conference on image and vision computing New Zealand (IVCNZ)*. IEEE, 2016, pp. 1–5.
- [3] M. A. Khan, T. M. Khan, T. A. Soomro, N. Mir, and J. Gao, "Boosting sensitivity of a retinal vessel segmentation algorithm," *Pattern Analysis and Applications*, vol. 22, pp. 583–599, 2019.
- [4] T. A. Soomro, T. M. Khan, M. A. Khan, J. Gao, M. Paul, and L. Zheng, "Impact of ica-based image enhancement technique on retinal blood vessels segmentation," *IEEE Access*, vol. 6, pp. 3524–3538, 2018.
- [5] M. A. Khan, T. M. Khan, D. G. Bailey, and T. A. Soomro, "A generalized multi-scale line-detection method to boost retinal vessel segmentation sensitivity," *Pattern Analysis and Applications*, vol. 22, pp. 1177–1196, 2019.
- [6] M. A. Khan, T. M. Khan, S. S. Naqvi, and M. Aurangzeb Khan, "Ggm classifier with multi-scale line detectors for retinal vessel segmentation," *Signal, Image and Video Processing*, vol. 13, pp. 1667–1675, 2019.
- [7] A. Khawaja, T. M. Khan, K. Naveed, S. S. Naqvi, N. U. Rehman, and S. J. Nawaz, "An improved retinal vessel segmentation framework using frangi filter coupled with the probabilistic patch based denoiser," *IEEE Access*, vol. 7, pp. 164 344–164 361, 2019.
- [8] A. Khawaja, T. M. Khan, M. A. Khan, and J. Nawaz, "A multi-scale directional line detector for retinal vessel segmentation," *Sensors*, vol. 19, no. 22, 2019.
- [9] M. A. Khan, T. M. Khan, K. I. Aziz, S. S. Ahmad, N. Mir, and E. Elbakush, "The use of fourier phase symmetry for thin vessel detection in retinal fundus images," in *2019 IEEE International Symposium on Signal Processing and Information Technology (ISSPIT)*. IEEE, 2019, pp. 1–6.
- [10] T. M. Khan, F. Abdullah, S. S. Naqvi, M. Arsalan, and M. A. Khan, "Shallow vessel segmentation network for automatic retinal vessel segmentation," in *2020 International Joint Conference on Neural Networks (IJCNN)*. IEEE, 2020, pp. 1–7.
- [11] T. M. Khan, S. S. Naqvi, M. Arsalan, M. A. Khan, H. A. Khan, and A. Haider, "Exploiting residual edge information in deep fully convolutional neural networks for retinal vessel segmentation," in *2020 International Joint Conference on Neural Networks (IJCNN)*. IEEE, 2020, pp. 1–8.
- [12] T. M. Khan, A. Robles-Kelly, and S. S. Naqvi, "A semantically flexible feature fusion network for retinal vessel segmentation," in *International Conference on Neural Information Processing*. Springer, Cham, 2020, pp. 159–167.
- [13] K. Naveed, F. Abdullah, H. A. Madni, M. A. Khan, T. M. Khan, and S. S. Naqvi, "Towards automated eye diagnosis: an improved retinal vessel segmentation framework using ensemble block matching 3d filter," *Diagnostics*, vol. 11, no. 1, p. 114, 2021.
- [14] F. Abdullah, R. Imtiaz, H. A. Madni, H. A. Khan, T. M. Khan, M. A. Khan, and S. S. Naqvi, "A review on glaucoma disease detection using computerized techniques," *IEEE Access*, vol. 9, pp. 37 311–37 333, 2021.
- [15] R. Imtiaz, T. M. Khan, S. S. Naqvi, M. Arsalan, and S. J. Nawaz, "Screening of glaucoma disease from retinal vessel images using semantic segmentation," *Computers & Electrical Engineering*, vol. 91, p. 107036, 2021.
- [16] S. J. Wiseman, J.-F. Zhang, C. Gray, C. Hamid, M. d. C. Valdés Hernández, L. Ballerini, M. J. Thrippleton, C. Manning, M. Stringer, E. Sleight *et al.*, "Retinal capillary microvessel morphology changes are associated with vascular damage and dysfunction in cerebral small vessel disease," *Journal of Cerebral Blood Flow & Metabolism*, vol. 43, no. 2, pp. 231–240, 2023.
- [17] N. Mirzaei, H. Shi, M. Oviatt, J. Doustar, A. Rentsendorj, D.-T. Fuchs, J. Sheyn, K. L. Black, Y. Koronyo, and M. Koronyo-Hamaoui, "Alzheimer's retinopathy: seeing disease in the eyes," *Frontiers in neuroscience*, vol. 14, p. 921, 2020.
- [18] T. M. Khan, A. Robles-Kelly, S. S. Naqvi, and A. Muhammad, "Residual multiscale full convolutional network (rm-fcn) for high resolution semantic segmentation of retinal vasculature," in *Structural, Syntactic, and Statistical Pattern Recognition: Joint IAPR International Workshops, S+SSPR 2020, Padua, Italy, January 21–22, 2021, Proceedings*. Springer Nature, 2021, p. 324.
- [19] T. M. Khan, M. A. Khan, N. U. Rehman, K. Naveed, I. U. Afridi, S. S. Naqvi, and I. Raazak, "Width-wise vessel bifurcation for improved retinal vessel segmentation," *Biomedical Signal Processing and Control*, vol. 71, p. 103169, 2022.
- [20] S. S. Naqvi, Z. A. Langah, H. A. Khan, M. I. Khan, T. Bashir, M. I. Razzak, and T. M. Khan, "Glan: Gan assisted lightweight attention network for biomedical imaging based diagnostics," *Cognitive Computation*, vol. 15, no. 3, pp. 932–942, 2023.
- [21] T. M. Khan, S. S. Naqvi, A. Robles-Kelly, and I. Razzak, "Retinal vessel segmentation via a multi-resolution contextual network and adversarial learning," *Neural Networks*, vol. 165, pp. 310–320, 2023.
- [22] T. M. Khan, S. Iqbal, S. S. Naqvi, I. Razzak, and E. Meijering, "Lmbfn: A lightweight multipath bidirectional focal attention network for multifeatures segmentation," in *2024 IEEE International Conference on Image Processing (ICIP)*. IEEE, 2024, pp. 2807–2813.
- [23] S. Iqbal, M. Zeeshan, M. Mehmood, T. M. Khan, and I. Razzak, "Tesl-net: A transformer-enhanced cnn for accurate skin lesion segmentation," *arXiv preprint arXiv:2408.09687*, 2024.
- [24] S. Iqbal, H. Ahmed, M. Sharif, M. Hena, T. M. Khan, and I. Razzak, "Euis-net: A convolutional neural network for efficient ultrasound image segmentation," *arXiv preprint arXiv:2408.12323*, 2024.
- [25] S. Iqbal, T. M. Khan, S. S. Naqvi, A. Naveed, and E. Meijering, "Tbconvl-net: A hybrid deep learning architecture for robust medical image segmentation," *Pattern Recognition*, vol. 158, p. 111028, 2025.
- [26] A. Naveed, S. S. Naqvi, T. M. Khan, S. Iqbal, M. Y. Wani, and H. A. Khan, "Ad-net: Attention-based dilated convolutional residual network with guided decoder for robust skin lesion segmentation," *Neural Computing and Applications*, pp. 1–23, 2024.
- [27] H. Farooq, Z. Zafar, A. Saadat, T. M. Khan, S. Iqbal, and I. Razzak, "Lssf-net: Lightweight segmentation with self-awareness, spatial attention, and focal modulation," *Artificial Intelligence in Medicine*, vol. 158, 2024.
- [28] U. Muhammad, R. Azka, S. Abdullah, R. Abd Ur, G. Sung-Min, L. Aleum, K. Tariq M., and R. Imran, "Advancing metaverse-based healthcare with multimodal neuroimaging fusion via multi-task adversarial variational autoencoder for brain age estimation," *IEEE Journal of Biomedical and Health Informatics*, pp. 1–9, 2024. [Online]. Available: <https://ieeexplore.ieee.org/document/10766589>
- [29] S. A. Burns, A. E. Elsner, and T. J. Gast, "Imaging the retinal vasculature," *Annual review of vision science*, vol. 7, pp. 129–153, 2021.
- [30] S. Iqbal, K. Naveed, S. S. Naqvi, A. Naveed, and T. M. Khan, "Robust retinal blood vessel segmentation using a patch-based statistical adaptive multi-scale line detector," *Digital Signal Processing*, vol. 139, p. 104075, 2023.
- [31] M. A. Manan, F. Jinchao, T. M. Khan, M. Yaqub, S. Ahmed, and I. s. Chuhan, "Semantic segmentation of retinal exudates using a residual encoder–decoder architecture in diabetic retinopathy," *Microscopy Research and Technique*, 2023.
- [32] M. Mehmood, M. Alsharari, S. Iqbal, I. Spence, and M. Fahim, "Retinalitenet: A lightweight transformer based cnn for retinal feature segmentation," in *Proceedings of the IEEE/CVF Conference on Computer Vision and Pattern Recognition (CVPR) Workshops*, June 2024, pp. 2454–2463.
- [33] T. M. Khan, M. Arsalan, S. Iqbal, I. Razzak, and E. Meijering, "Feature enhancer segmentation network (fes-net) for vessel segmentation," in *2023 International Conference on Digital Image Computing: Techniques and Applications (DICTA)*. IEEE, 2023, pp. 160–167.
- [34] M. M. Abbasi, S. Iqbal, A. Naveed, T. M. Khan, S. S. Naqvi, and W. Khalid, "Lmbis-net: A lightweight multipath bidirectional skip connection based cnn for retinal blood vessel segmentation," *arXiv preprint arXiv:2309.04968*, 2023.
- [35] S. Iqbal, T. M. Khan, S. S. Naqvi, A. Naveed, M. Usman, H. A. Khan, and I. Razzak, "Ldmres-net: A lightweight neural network for efficient medical image segmentation on iot and edge devices," *IEEE journal of biomedical and health informatics*, 2023.
- [36] M. Mehmood, T. M. Khan, M. A. Khan, S. S. Naqvi, and W. Alhalabi, "Vessel intensity profile uniformity improvement for retinal vessel segmentation," *Procedia Computer Science*, vol. 163, pp. 370–380, 2019.
- [37] M. Matloob Abbasi, S. Iqbal, K. Aurangzeb, M. Alhusein, and T. M. Khan, "Lmbis-net: A lightweight bidirectional skip connection based multipath cnn for retinal blood vessel segmentation," *Scientific Reports*, vol. 14, no. 1, p. 15219, 2024.
- [38] S. Javed, T. M. Khan, A. Qayyum, A. Sowmya, and I. Razzak, "Region guided attention network for retinal vessel segmentation," *arXiv preprint arXiv:2407.18970*, 2024.

- [39] S. Iqbal, T. M. Khan, K. Naveed, S. S. Naqvi, and S. J. Nawaz, "Recent trends and advances in fundus image analysis: A review," *Computers in Biology and Medicine*, vol. 151, p. 106277, 2022.
- [40] T. M. Khan, A. Robles-Kelly, and S. S. Naqvi, "Rc-net: A convolutional neural network for retinal vessel segmentation," in *2021 Digital Image Computing: Techniques and Applications (DICTA)*. IEEE, 2021, pp. 01–07.
- [41] T. M. Khan, S. S. Naqvi, and E. Meijering, "Leveraging image complexity in macro-level neural network design for medical image segmentation," *Scientific Reports*, vol. 12, no. 1, p. 22286, 2022.
- [42] T. M. Khan, A. Robles-Kelly, and S. S. Naqvi, "T-net: A resource-constrained tiny convolutional neural network for medical image segmentation," in *Proceedings of the IEEE/CVF winter conference on applications of computer vision*, 2022, pp. 644–653.
- [43] S. Iqbal, S. Naqvi, H. Ahmed, A. Saadat, and T. M. Khan, "G-net light: A lightweight modified google net for retinal vessel segmentation," in *Photonics*, vol. 9, no. 12. MDPI, 2022, pp. 923–936.
- [44] M. Arsalan, T. M. Khan, S. S. Naqvi, M. Nawaz, and I. Razzak, "Prompt deep light-weight vessel segmentation network (plvs-net)," *IEEE/ACM Transactions on Computational Biology and Bioinformatics*, vol. 20, no. 2, pp. 1363–1371, 2022.
- [45] T. M. Khan, M. Arsalan, A. Robles-Kelly, and E. Meijering, "Mkis-net: a light-weight multi-kernel network for medical image segmentation," in *International Conference on Digital Image Computing: Techniques and Applications (DICTA)*. 10.1109/DICTA56598.2022.10034573, 2022, pp. 1–8.
- [46] J. Yang, C. Li, X. Dai, and J. Gao, "Focal modulation networks," *Advances in Neural Information Processing Systems*, vol. 35, pp. 4203–4217, 2022.
- [47] H. Wang, Z. Wang, M. Jia, A. Li, T. Feng, W. Zhang, and L. Jiao, "Spatial attention for multi-scale feature refinement for object detection," in *Proceedings of the IEEE/CVF International Conference on Computer Vision Workshops*, 2019, pp. 0–0.
- [48] T. A. Qureshi, M. Habib, A. Hunter, and B. Al-Diri, "A manually-labeled, artery/vein classified benchmark for the drive dataset," in *Proceedings of the 26th IEEE international symposium on computer-based medical systems*. IEEE, 2013, pp. 485–488.
- [49] J. Zhang, B. Dashtbozorg, E. Bekkers, J. P. W. Pluim, R. Duits, and B. M. ter Haar Romeny, "Robust retinal vessel segmentation via locally adaptive derivative frames in orientation scores," *IEEE Transactions on Medical Imaging*, vol. 35, no. 12, pp. 2631–2644, Dec 2016.
- [50] A. Hoover, V. Kouznetsova, and M. Goldbaum, "Locating blood vessels in retinal images by piecewise threshold probing of a matched filter response," *IEEE Transactions Medical Imaging*, vol. 19, no. 3, pp. 203–210, 2000.
- [51] A. E. Chowdhury, G. Mann, W. H. Morgan, A. Vukmirovic, A. Mehnert, and F. Sohel, "Msganet-rav: A multiscale guided attention network for artery-vein segmentation and classification from optic disc and retinal images," *Journal of optometry*, vol. 15, pp. S58–S69, 2022.
- [52] R. Hemelings, B. Elen, I. Stalmans, K. Van Keer, P. De Boever, and M. B. Blaschko, "Artery-vein segmentation in fundus images using a fully convolutional network," *Computerized Medical Imaging and Graphics*, vol. 76, p. 101636, 2019.
- [53] X. Lyu, P. Jajal, M. Z. Tahir, and S. Zhang, "Fractal dimension of retinal vasculature as an image quality metric for automated fundus image analysis systems," *Scientific Reports*, vol. 12, p. 11868, 2022.
- [54] Y. Xu and Y. Fan, "Dual-channel asymmetric convolutional neural network for an efficient retinal blood vessel segmentation in eye fundus images," *Biocybernetics and Biomedical Engineering*, vol. 42, no. 2, pp. 695–706, 2022.
- [55] A. Dosovitskiy, L. Beyer, A. Kolesnikov, D. Weissenborn, X. Zhai, T. Unterthiner, M. Dehghani, M. Minderer, G. Heigold, S. Gelly, J. Uszkoreit, and N. Houlsby, "An image is worth 16x16 words: Transformers for image recognition at scale," *arXiv:2010.11929*, 2020.
- [56] B. Zhang, Z. Tian, Q. Tang, X. Chu, X. Wei, C. Shen, and Y. Liu, "SegViT: Semantic segmentation with plain vision transformers," *arXiv:2210.05844*, 2022.
- [57] S. Zheng, J. Lu, H. Zhao, X. Zhu, Z. Luo, Y. Wang, Y. Fu, J. Feng, T. Xiang, P. H. Torr, and L. Zhang, "Rethinking semantic segmentation from a sequence-to-sequence perspective with transformers," in *IEEE/CVF Conference on Computer Vision and Pattern Recognition (CVPR)*, 2021, pp. 6881–6890.
- [58] R. Strudel, R. Garcia, I. Laptev, and C. Schmid, "Segmenter: Transformer for semantic segmentation," in *IEEE/CVF International Conference on Computer Vision (ICCV)*, 2021, pp. 7262–7272.
- [59] R. Ranftl, A. Bochkovskiy, and V. Koltun, "Vision transformers for dense prediction," in *IEEE/CVF International Conference on Computer Vision (ICCV)*, 2021, pp. 12 179–12 188.
- [60] W. Liu, H. Yang, T. Tian, Z. Cao, X. Pan, W. Xu, Y. Jin, and F. Gao, "Full-resolution network and dual-threshold iteration for retinal vessel and coronary angiograph segmentation," *IEEE journal of biomedical and health informatics*, vol. 26, no. 9, pp. 4623–4634, 2022.
- [61] Z. Zhang, C. Wu, S. Coleman, and D. Kerr, "DENSE-INception U-net for medical image segmentation," *Computer Methods and Programs in Biomedicine*, vol. 192, p. 105395, 2020.
- [62] F. Isensee, P. F. Jaeger, S. A. Kohl, J. Petersen, and K. H. Maier-Hein, "nnU-Net: a self-configuring method for deep learning-based biomedical image segmentation," *Nature Methods*, vol. 18, no. 2, pp. 203–211, 2021.
- [63] T. Lei, W. Zhou, Y. Zhang, R. Wang, H. Meng, and A. K. Nandi, "Lightweight V-Net for liver segmentation," in *IEEE International Conference on Acoustics, Speech and Signal Processing (ICASSP)*, 2020, pp. 1379–1383.
- [64] T. Tarasiewicz, M. Kawulok, and J. Nalepa, "Lightweight U-Nets for brain tumor segmentation," in *International MICCAI Brain Lesion Workshop*, 2020, pp. 3–14.
- [65] C. Li, Y. Fan, and X. Cai, "PyConvU-Net: A lightweight and multiscale network for biomedical image segmentation," *BMC Bioinformatics*, vol. 22, no. 1, pp. 1–11, 2021.
- [66] A. G. Howard, M. Zhu, B. Chen, D. Kalenichenko, W. Wang, T. Weyand, M. Andreetto, and H. Adam, "MobileNets: Efficient convolutional neural networks for mobile vision applications," *arXiv:1704.04861*, 2017.
- [67] J. Morano, Á. S. Hervella, J. Novo, and J. Rouco, "Simultaneous segmentation and classification of the retinal arteries and veins from color fundus images," *Artificial Intelligence in Medicine*, vol. 118, p. 102116, 2021.
- [68] D. Shi, S. He, J. Yang, Y. Zheng, and M. He, "One-shot retinal artery and vein segmentation via cross-modality pretraining," *Ophthalmology Science*, vol. 4, no. 2, p. 100363, 2024.
- [69] J. Fhima, J. Van Eijgen, H. Kulenovic, V. Debeuf, M. Vangilbergen, M.-I. Billen, H. Brackenier, M. Freiman, I. Stalmans, and J. A. Behar, "Lunet: deep learning for the segmentation of arterioles and venules in high resolution fundus images," *Physiological Measurement*, 2024.
- [70] J. Hu, H. Wang, G. Wu, Z. Cao, L. Mou, Y. Zhao, and J. Zhang, "Multi-scale interactive network with artery/vein discriminator for retinal vessel classification," *IEEE Journal of Biomedical and Health Informatics*, vol. 26, no. 8, pp. 3896–3905, 2022.
- [71] W. Ma, S. Yu, K. Ma, J. Wang, X. Ding, and Y. Zheng, "Multi-task neural networks with spatial activation for retinal vessel segmentation and artery/vein classification," in *Medical Image Computing and Computer Assisted Intervention—MICCAI 2019: 22nd International Conference, Shenzhen, China, October 13–17, 2019, Proceedings, Part I 22*. Springer, 2019, pp. 769–778.
- [72] X. Li, Y. Jiang, M. Li, and S. Yin, "Lightweight attention convolutional neural network for retinal vessel image segmentation," *IEEE Transactions on Industrial Informatics*, vol. 17, no. 3, pp. 1958–1967, 2020.
- [73] C. Chen, J. H. Chuah, R. Ali, and Y. Wang, "Retinal vessel segmentation using deep learning: a review," *IEEE Access*, vol. 9, pp. 111 985–112 004, 2021.
- [74] Q. Hu, M. D. Abràmoff, and M. K. Garvin, "Automated separation of binary overlapping trees in low-contrast color retinal images," in *Medical Image Computing and Computer-Assisted Intervention—MICCAI 2013: 16th International Conference, Nagoya, Japan, September 22–26, 2013, Proceedings, Part II 16*. Springer, 2013, pp. 436–443.
- [75] O. Ronneberger, P. Fischer, and T. Brox, "U-Net: Convolutional networks for biomedical image segmentation," in *International Conference on Medical Image Computing and Computer-Assisted Intervention (MICCAI)*, 2015, pp. 234–241.
- [76] O. Oktay, J. Schlemper, L. L. Folgoc, M. Lee, M. Heinrich, K. Misawa, K. Mori, S. McDonagh, N. Y. Hammerla, B. Kainz *et al.*, "Attention u-net: Learning where to look for the pancreas," *arXiv preprint arXiv:1804.03999*, 2018.
- [77] N. Ibtehaz and M. S. Rahman, "Multiresunet: Rethinking the u-net architecture for multimodal biomedical image segmentation," *Neural networks*, vol. 121, pp. 74–87, 2020.
- [78] R. Azad, M. Asadi-Aghbolaghi, M. Fathy, and S. Escalera, "Bi-directional convlstm u-net with densely connected convolutions," in *Proceedings of the IEEE/CVF international conference on computer vision workshops*, 2019, pp. 0–0.
- [79] V. Badrinarayanan, A. Kendall, and R. Cipolla, "Segnet: A deep convolutional encoder-decoder architecture for image segmentation," *IEEE transactions on pattern analysis and machine intelligence*, vol. 39, no. 12, pp. 2481–2495, 2017.

- [80] Z. Zhou, M. M. Rahman Siddiquee, N. Tajbakhsh, and J. Liang, "UNet++: A nested u-net architecture for medical image segmentation," in *International Workshops on Deep Learning in Medical Image Analysis (DLMA) and Multimodal Learning for Clinical Decision Support (ML-CDS) Held in Conjunction with MICCAI*, 2018, pp. 3–11.
- [81] M. Mehmood, M. Alsharari, S. Iqbal, I. Spence, and M. Fahim, "Retinalitenet: A lightweight transformer based cnn for retinal feature segmentation," in *Proceedings of the IEEE/CVF Conference on Computer Vision and Pattern Recognition*, 2024, pp. 2454–2463.
- [82] M. M. Fraz, P. Remagnino, A. Hoppe, B. Uyyanonvara, A. R. Rudnicka, C. G. Owen, and S. A. Barman, "An ensemble classification-based approach applied to retinal blood vessel segmentation," *IEEE Transactions on Biomedical Engineering*, vol. 59, no. 9, pp. 2538–2548, 2012.